Journal of Membrane Science 565 (2018) 390–401

Contents lists available at ScienceDirect

Journal of Membrane Science

journal homepage: www.elsevier.com/locate/memsci

Study on the formation of thin film nanocomposite (TFN) membranes of polymers of intrinsic microporosity and graphene-like fillers: Effect of lateral flake size and chemical functionalization

Monica Alberto[a], Rupesh Bhavsar[b], Jose Miguel Luque-Alled[a], Eric Prestat[c,d], Lei Gao[b], Peter M. Budd[b], Aravind Vijayaraghavan[c], Gyorgy Szekely[a], Stuart M. Holmes[a], Patricia Gorgojo[a,*]

[a] School of Chemical Engineering and Analytical Science, The University of Manchester, United Kingdom
[b] School of Chemistry, The University of Manchester, United Kingdom
[c] School of Materials, The University of Manchester, United Kingdom
[d] SuperSTEM Laboratory, SciTech Daresbury Campus, United Kingdom

ARTICLE INFO

Keywords:
Alkyl functionalization
Graphene oxide
Polymer of intrinsic microporosity PIM-1
Thin film nanocomposite membranes
Pervaporation

ABSTRACT

Thin film nanocomposite (TFN) membranes of polymer of intrinsic microporosity PIM-1 incorporating graphene oxide (GO) nanosheets of different sizes and chemistries are presented. These membranes show an improved separation performance for the recovery of *n*-butanol from aqueous solutions through pervaporation; an improvement of ca. a third of the value achieved for pristine PIM-1 thin films is obtained for TFN membranes filled with nanometer-sized reduced octyl-functionalized GO. In addition, these nanometer-sized fillers lead to a maximum increase in total flux of approximately 40%. The thickness of the supported films is in the range 1–1.5 μm, and fillers used are micrometer- and nanometer-sized alkyl-functionalized GO nanosheets and their chemically reduced counterparts. As evidenced by a superior overall membrane performance, the interfacial interaction between the filler and the polymer matrix is enhanced for those whose lateral size is in the nanometer range. Moreover, an enhancement in the separation performance and productivity of such membranes is observed for higher operating temperatures and higher contents of *n*-butanol in the feed.

1. Introduction

Pervaporation (PV) is a membrane-based technology that can potentially replace energy-intensive distillation processes currently used for industrial separation such as the recovery of bioalcohols from fermentation broths. Bioalcohols are established as sustainable alternatives to fossil fuels, but there are hurdles to be overcome in the development of effective membrane materials for their separation. For instance, polymer membranes show a trade-off between permeability and selectivity and typically undergo swelling when exposed to organic solvents. Inorganic membranes, on the other hand, are brittle and can get damaged more easily. In addition, other considerations regarding the economic viability of the technology need to be made; polymers are inexpensive to process, whereas the cost of processing inorganic materials is high but they stand out for their high thermal and chemical stability, and higher selectivity [1,2].

The flux through a membrane is directly proportional to the reciprocal of the membrane thickness. Therefore, in recent years extensive research has been geared towards the preparation of extremely thin layers with molecular separation properties, using 2-dimensional inorganic materials: high-aspect-ratio zeolites [3], carbon materials such as diamond-like carbon nanosheets [4], graphene oxide (GO) [5–11] and reduced graphene oxide (rGO) [12–15]. However, large-scale preparation of such membranes is a challenge.

Mixed matrix membranes (MMMs), composed of particles of diverse nature incorporated in polymeric matrices, seem to be good candidates to benefit from the advantageous properties of both types of material. Porous materials (zeolites [16,17], metal-organic frameworks (MOFs) [18,19], and carbon nanotubes (CNTs) [20,21]) and non-porous materials (graphene [22]) have been used as fillers in MMMs. However, large loadings are often needed in order to achieve noticeable improvements in the separation performance as compared to the pristine polymers, which increases the cost and gives rise to problems of agglomeration and formation of non-selective voids. Moreover, most of

* Corresponding author.
E-mail address: p.gorgojo@manchester.ac.uk (P. Gorgojo).

https://doi.org/10.1016/j.memsci.2018.08.050
Received 17 May 2018; Received in revised form 25 July 2018; Accepted 25 August 2018
Available online 28 August 2018

the research on MMMs deals with freestanding membranes that are several tens of microns thick, which are unviable for industrial applications [17,23,24].

Whether it is a purely polymeric membrane or a MMM, it should be produced as a thin dense selective layer supported on a much cheaper and thicker porous substrate, so as to maximize the flux of permeate and minimize the area required to process large-scale streams [25]. This arrangement also brings down the cost of the membrane, since the amount of active material can be considerably reduced. The dense thin layer can be a few tens or hundreds of nanometers in thickness, and when separately formed on top of the porous support (tens of microns thick) the combination is referred to as a thin film composite (TFC) membrane. When nanoparticles are embedded in the polymer thin layer, the configuration is known as a thin film nanocomposite (TFN) membrane. Both TFC and TFN membranes are typically produced via techniques such as coating or interfacial polymerization.

Polyamide TFC membranes used for reverse osmosis and for nanofiltration in organic liquids are produced via interfacial polymerization (IP) and comprise an active polyamide layer of about 200 nm in thickness. Recently, this thickness has been lowered down to a sub-10 nm film by controlling the interfacial reaction, and the resulting membranes have shown permeance values two orders of magnitude higher than commercial ones [26]. Similarly, ultrathin polyarylate nanofilms with thicknesses down to 20 nm have been synthesized via IP [27]. Other successful attempts to increase the flux through thin film polyamide membranes include the addition of porous MOF nanoparticles in the polyamide layer during the IP reaction [28–30]. Graphene-like materials have also been introduced into thin film polyamide membranes to enhance their separation performance and provide them with anti-fouling properties [31–33]. Polyamide films are hydrophilic and can be used for the dehydration of alcohols [34,35]. However, for the recovery of alcohols from fermentation broths, where the alcohol concentration can be as low as 2 wt% [36], organophilic membranes are required.

Polymers of intrinsic microporosity (PIMs) are a class of organophilic material with exceptional separation properties, not just in terms of selectivity but also in terms of permeability (i.e. flux normalized for the driving force and the membrane thickness). The first membrane-forming PIM to be synthesized, PIM-1, has been used for gas separation [37–39], pervaporation [40,41] and organic solvent nanofiltration [42]. To date, thin films of PIM-1 have been prepared on porous supports via dip coating [22,43] and spin coating/transferal [42]. Very recently integrally skinned asymmetric (ISA) PIM-1 hollow fibers have been reported for the first time [44]. ISA membranes, like TFC membranes, comprise a thin dense separation layer supported on a highly porous structure, produced in this case via immersion precipitation. Thus, the dense and the porous structures are both produced in a single step from the same polymer solution, which makes the structure more stable as compared to a TFC. However, large amounts of expensive PIM-1 are needed for producing ISA membranes, as compared to supported TFCs [45].

Freestanding PIM-1 membranes several tens of microns thick have been investigated for *n*-butanol recovery from aqueous solutions [22,46]. In our previous study, the separation performance of PIM-1 freestanding membranes (~ 60 μm in thickness) was greatly improved by adding alkyl-functionalized graphene oxide into the polymer matrix due to the enhanced membrane affinity towards n-butanol and decreased affinity towards water. The best membrane showed a 144% increase in the separation factor for *n*-butanol with a total flux of 1.2 kg m^{-2} h^{-1}, but that is still low, as expected for freestanding membranes [22]. Furthermore, polyvinylidine fluoride (PVDF) porous supports were investigated for the preparation of TFC membranes via dip coating (thickness of pristine PIM-1 active layer in the range 1.0–2.9 μm) and flux values of up to 9.08 kg m^{-2} h^{-1} were reported [47]. Herein, thin film nanocomposite (TFN) membranes made with PIM-1 incorporated with alkyl-functionalized GO nanosheets are prepared on PVDF supports for *n*-butanol/water separation. Considering that contradicting results on MMMs have been reported in the literature [17,23,24,48–50], the effect of the filler size and loading on the membrane performance is investigated in this study. In addition, the effect of operating temperature and feed composition on the PV performance of the membranes with optimal fillers is also analyzed. Optimizing the size and concentration of fillers in TFN membranes is essential for achieving good separation performance and therefore, positioning them as candidates for the next generation of commercial membranes, where high flux and separation performance are critical.

2. Experimental section

2.1. Materials

Polyvinylidene fluoride (PVDF, Mw ~5.34×10^5 g mol^{-1}), dimethylacetamide (DMAc), chloroform, *n*-butanol, octadecylamine (ODA), octylamine (OA), dichloromethane (DCM), hydrazine monohydrate (~80 vol% in H_2O) and phosphoric acid were purchased from Sigma Aldrich (UK). Non-woven fabric (2471 Polypropylene/Polyethylene (PP/PE)) was purchased from Freudenberg-Filter, Germany. Graphite was purchased from NGS Naturegraphit GmbH (Germany). Potassium permanganate and 5,5′,6,6′-tetrahydroxy-3,3,3′,3′-tetramethyl-1,1′-spirobisindane (TTSBI) were acquired from Alfa Aesar (UK). Ammonia was procured from Acros Organics (United Kingdom). Toluene, methanol, potassium hydroxide and TFTPN (tetrafluoroterephthalonitrile) were purchased from Sigma Aldrich. TTSBI was dissolved in methanol and precipitated in DCM before use. TFTPN was purified through sublimation at 150 °C and then collected without vacuum. All the other chemicals were used as obtained without any purification. Commercial PERVAP 4060 membranes were kindly supplied by DeltaMem AG, Switzerland.

2.2. Synthesis and characterization of PIM-1

PIM-1 was prepared as described by Du et al. [51]. Its average molecular weight was determined through gel permeation chromatography (GPC) on a multi-detector Viscotek GCPmax VE 2001 chromatograph (Malvern, UK), equipped with two PL gel mixed-B columns and Viscotek TDA302 triple detector array. Analysis was performed in chloroform at a flow rate of 1 mL min^{-1}. OmniSEC software (Malvern, UK) was used to analyze the data. The polymer was dissolved in chloroform at a concentration of 1 mg mL^{-1}.

2.3. Synthesis of alkyl-functionalized GO fillers

GO was synthetized through a modified Hummers' method [52], and was further functionalized with two alkylamines of different lengths – octylamine (OA) and octadecylamine (ODA) and reduced as reported previously [22]. Solutions of GO-ODA, rGO-ODA and rGO-OA dispersed in chloroform were probe sonicated for 10 min and 8 h (Cole-Parmer, 750 W, 20 kHz, amplitude 22% - Cole-Parmer Instrument, USA) in discontinuous mode (pulse on for 9 s and pulse off for 9 s) in order to achieve graphene-like flakes with different lateral sizes. During probe sonication, an ice bath was used to avoid an increase in temperature. Fig. S1 shows a schematic diagram of the synthesis of the graphene-like materials.

2.4. Preparation and characterization of PVDF membrane supports

PVDF supports were prepared by phase inversion technique as described in the work by Gao et al. [47] with the casting solution containing 18 wt% PVDF, 3 wt% phosphoric acid and 79 wt% DMAc. Dope solutions were stirred at approximately 70 °C for about 15 h, until a homogeneous solution was obtained and were subsequently left without stirring overnight to remove air bubbles. The viscosity of the

PVDF dope solution was measured using an Elcometer 2300 Rotational Viscometer (Elcometer Limited, UK), using a TL7 spindle and a spindle speed of 6 rpm. The measurement was done at a humidity and temperature of 65% and 20.3 °C, respectively, and gave a value of 5390 mPa s. An automatic film applicator (Sheen 1133 N, UK) was used for the casting, with the knife set at 250 µm and the speed at 0.05 m s^{-1}. After casting, the membranes were immersed into a DI water bath at room temperature for about 10 min and then kept in another water bath until they were dried at room temperature the day prior to be use for the preparation of the composite membranes. The mean pore size of the support was calculated by the gas permeation method used by Fontananova et al. [53]. Details on this method are presented in the supporting information.

2.5. Preparation of dip-coated thin film nanocomposite membranes

TFN membranes supported on porous PVDF were prepared through a dip-coating technique using an in-house built system. The polymer content used in all coating solutions was 4 wt% in chloroform; whereas the filler loading ranged from 0.01 to 0.25 wt% with regards to the weight of the polymer. PVDF membrane supports were dried at room temperature overnight before use and cut into a rectangular shape (~ 3 cm x 10 cm). TFN membranes were prepared by putting the PVDF supports in contact with the coating solutions for 0.7 s, as schematized in Fig. 1.

2.6. Characterization of GO and alkyl-functionalized GO

GO, GO-ODA, rGO-ODA and rGO-OA were characterized using attenuated total reflectance Fourier transform infrared spectroscopy (ATR-FTIR), Raman spectroscopy, thermogravimetric analysis (TGA) and atomic force microscopy (AFM) as in our previous work [22]. The lateral flake size of the nanosheets was analyzed by SEM using a SEM FEI Quanta 250 FEG-SEM (FEI, USA). For that, GO was dispersed in water and spin-coated onto a silicon dioxide wafer. GO-ODA, rGO-ODA and rGO-OA were dispersed in chloroform and then spray-coated onto a silicon dioxide wafer.

2.7. Membrane characterization

A Quanta 250FEG-SEM (FEI, USA) was used to observe cross sections and surfaces of the TFN membranes. The samples were immersed firstly in ethanol for about 30 s and then in liquid nitrogen for another 30 s where they were fractured. Subsequently, they were coated with a conductive layer of sputtered Platinum. ImageJ (NIH) open-source software was used to determine the mean pore size and surface porosity of the PVDF membranes from the SEM images, as well as to determine the thickness of the TFN dense layer formed on top of the PVDF membrane supports. Scanning Transmission Electron Microscopy (STEM) and Electron Diffraction (ED) data were collected using a FEI Titan 80–200 equipped with a Chemistem EDX detector, probe-side aberration corrector and an X-FEG electron source operating at 200 kV. In STEM mode, the microscope was set at a beam current of 100 pA, and a convergence angle of 21 mrad and collection angles ranging from 0 to 14 mrad for the bright field detector. Electron diffraction pattern were acquired over an area of 0.2 µm2 using the smallest condenser aperture (50 µm diameter) of the microscope. For TEM specimen preparation, the membranes were embedded in TAAB 812 epoxy resin (TAAB Laboratories, UK) that was allowed to polymerize at 60 °C for 24 h. Ultrathin sections (80 nm) were then obtained using an ultracut E ultramicrotome (Reichert-Jung, USA). The face of the membrane was positioned perpendicular to the edge of the diamond knife (DiATOME, Switzerland) allowing cross sections of the specimen to be acquired, which were collected on to copper Lacey carbon film (Agar Scientific Ltd, UK).

UV–Visible spectroscopy was used to determine the filler concentration in the PIM-1/graphene coating solutions. Part of the solution used for dip coating was dried at room temperature and subsequently placed in the vacuum oven in order to remove any residual solvent. Afterwards, dried samples were weighed and redissolved in chloroform (4 mL). At least three samples of each coating solution were measured. The absorbance at 660 nm was recorded using a Genesys 10 S UV–Vis spectrophotometer (Thermo Scientific, United Kingdom), using av-quartz cuvette with a 1 cm optical path at room temperature. The extinction coefficients obtained in our previous work were used; 4.939, 15.256, and 7.556 mL mg^{-1} cm^{-1} for GO-ODA, rGO-ODA, and rGO-OA, respectively [22].

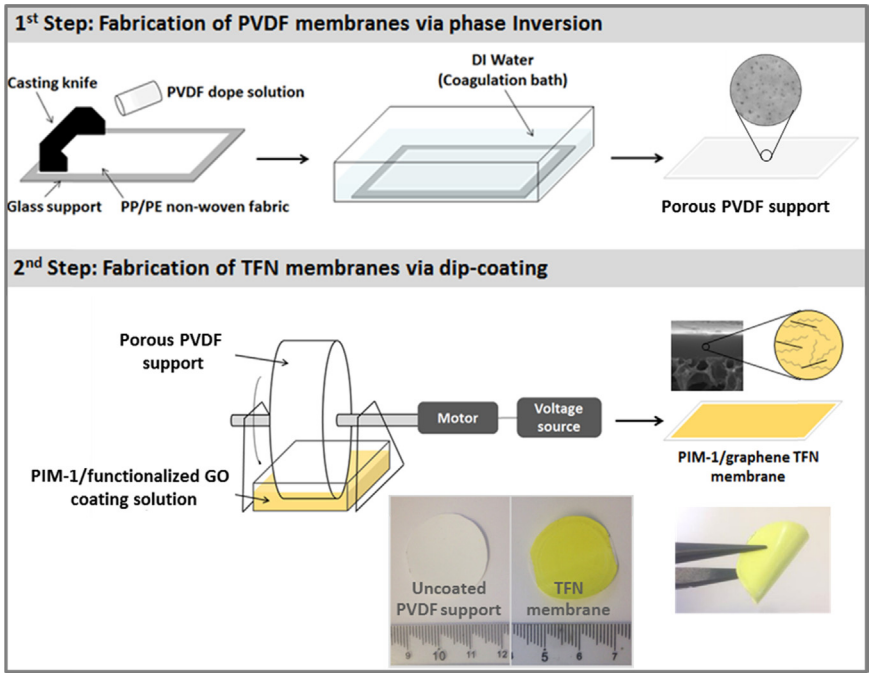

Fig. 1. Schematic representation of the fabrication process of the thin film nanocomposite (TFN) membranes. It includes a first step of fabrication of porous supports via phase inversion, and a second step of coating such supports with PIM-1 solutions containing alkyl-functionalized graphene oxide nanosheets. Pictures of an uncoated PVDF support disc and a TFN membrane disc are displayed; the scale bar is in cm.

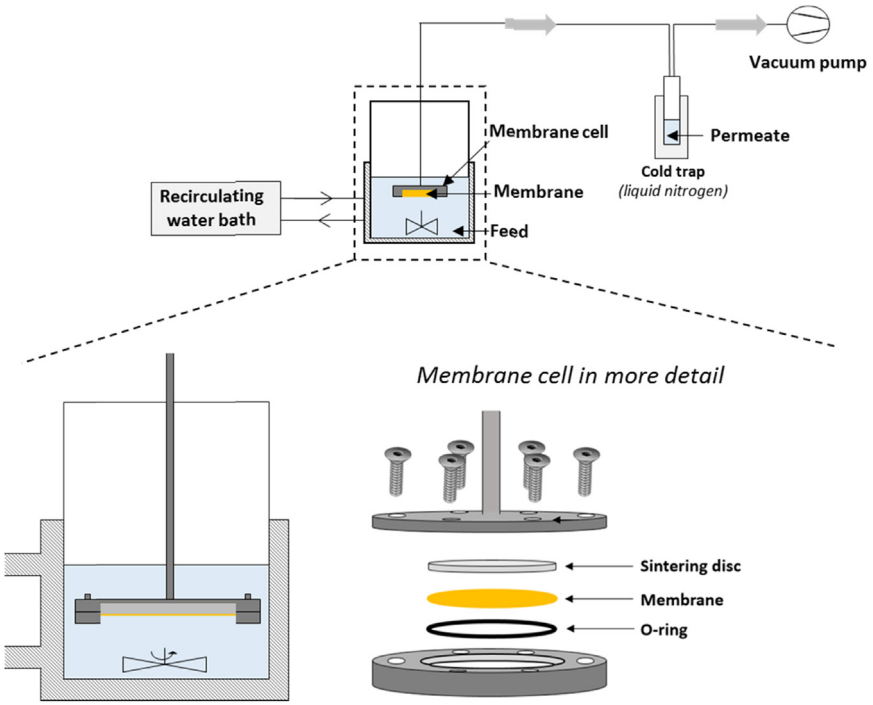

Fig. 2. Setup used for carrying out the PV tests and detailed scheme of the PV cell.

2.8. Separation of n-butanol/water via pervaporation

PV was carried out as described in our previous work on free-standing membranes [22]. The PV laboratory apparatus used to test the prepared membranes is represented in Fig. 2. All membranes were initially tested at 65 °C using an aqueous binary mixture containing 5 wt% of *n*-Butanol. In addition, the effect of the temperature and composition of the feed solution on the separation performance was investigated for membranes 0.05GO-ODA-S, 0.05rGO-ODA-S and 0.05rGO-OA-S. For these membranes, the temperature was varied from 35 to 65 °C using a binary mixture of 5 wt% *n*-Butanol. The effect of the feed composition was also studied by varying the *n*-Butanol composition from 2 to 5 wt% at a constant temperature of 65 °C. The effective area of the membranes was 2.54 cm^2. The downstream pressure was 10 mbar. The permeate flux, J, (kg m^{-2} h^{-1}) was determined using Eq. (1):

$$J = \frac{m}{At} \quad (1)$$

where m is the weight of the permeate (kg), A is the effective membrane area (m^2) in contact with the feed solution and t is the permeate collection time (h). The separation factor, β, was determined as in Eq. (2):

$$\beta = \frac{Y_{butanol}/Y_{water}}{X_{butanol}/X_{water}} \quad (2)$$

where $Y_{butanol}/Y_{water}$ is the weight ratio of *n*-butanol to water in the permeate and $X_{butanol}/X_{water}$ is the corresponding ratio in the feed.

Commercial PERVAP 4060 membranes were also tested for *n*-butanol recovery from aqueous solutions under the same conditions.

3. Results and discussion

TFN membranes were prepared via dip coating of alkyl-functionalized GO nanosheets dispersed in a solution of PIM-1 in chloroform (nanosheet concentrations of 0.01–0.25 wt% with regards to the mass of PIM-1) onto tailored porous PVDF supports, with active layer thicknesses as low as 1 μm, as schematized in Fig. 1. Dip coating was the selected technique as it can produce reasonable defect-free thin layers than can be scaled up for the production of larger amounts of membranes for industrial applications. However, some challenges were encountered when moving from a freestanding configuration (such as that previously reported [22]) to a much thinner supported membrane: (i) appropriate porous substrates onto which the thin films are fabricated were tailored (high surface porosity and small pore size) and (ii) nanosheets with suitable sizes had to be selected in order to avoid inhomogeneity and defects within the selective thin film. In this work three different fillers were used for the preparation of TFN membranes: GO functionalized using octadecylamine (GO-ODA) and its chemically reduced form (rGO-ODA), and GO functionalized using octylamine then chemically reduced (rGO-OA). The lateral size of the flakes was reduced via sonication and its effect on the membrane performance was studied.

3.1. Lateral size of alkyl-functionalized graphene oxide nanosheets

Samples of GO-ODA, rGO-ODA and rGO-OA were dispersed in chloroform and probe sonicated at different times, 10 min and 8 h, in order to obtain flakes with maximum lateral sizes of few micrometers and few hundreds of nanometer, respectively. The size distribution of the nanosheets was characterized via direct image analysis from scanning electron microscope (SEM) images. Fig. 3 shows micrographs of the fillers and their lateral flake size distributions, which were derived from between 70 and 147 flakes. Gaussian curve-fitting was used to determine the mean value for each individual sample. According to these results, after probe sonicating for 10 min, the average lateral flake sizes of GO-ODA, rGO-ODA and rGO-OA were 0.74 ± 0.40 μm, 1.26 ± 0.75 μm and 1.35 ± 0.73 μm, respectively. After a longer probe sonication of 8 h the average lateral flake size decreased to 0.25 ± 0.16 μm, 0.25 ± 010 μm and 0.26 ± 0.16 μm for GO-ODA, rGO-ODA and rGO-OA, respectively.

3.2. Characterization of PVDF membrane supports

The surface and cross-section of the PVDF membrane support used for the TFN membrane preparation is shown in Fig. S2 in the supporting information. Phosphoric acid was added to the casting solution in order to enhance the surface porosity and decrease the average pore size of the polymer supports. This is desirable for the formation of defect-free

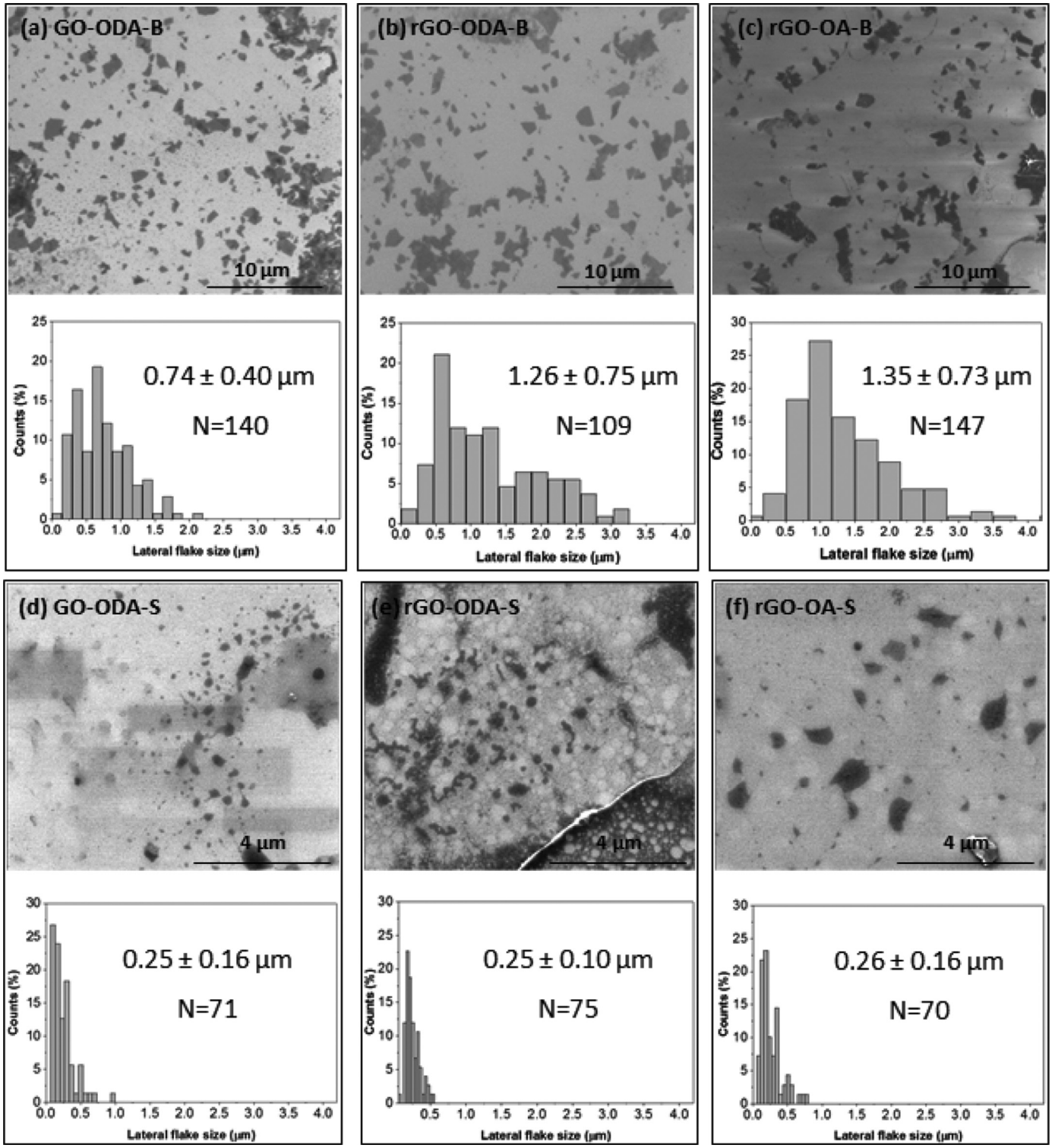

Fig. 3. SEM images of graphene-like nanosheets probe sonicated in chloroform for 10 min (a) GO-ODA-B, (b) rGO-ODA-B and (c) rGO-OA10-B, and flakes probe sonicated in chloroform for 8 h (d) GO-ODA-S, (e) rGO-ODA-S and (f) rGO-OA-S. Distributions of the lateral sizes are shown below each micrograph. *N* corresponds to the number of flakes that were analyzed.

TFN membranes with sufficiently high flux values, as previously reported [47]. From the analysis of the SEM images, the surface porosity and average pore size obtained were in the range 4.2–11.7% and 64 ± 31 nm, respectively. The mean pore size calculated via the gas permeation method shown in the supporting information (Fig. S3) was 34 nm which falls in the range of values obtained by SEM.

The surface topology of the PVDF membrane support was also investigated through AFM (Fig. S4). Areas of 30 × 30 µm were examined and the roughness parameters were calculated; the average roughness profile (R_a) value was 35.4 ± 1.2 nm, whereas the average root mean square roughness (R_q) value was 44.9 ± 1.6 nm, in accordance to reported values [47].

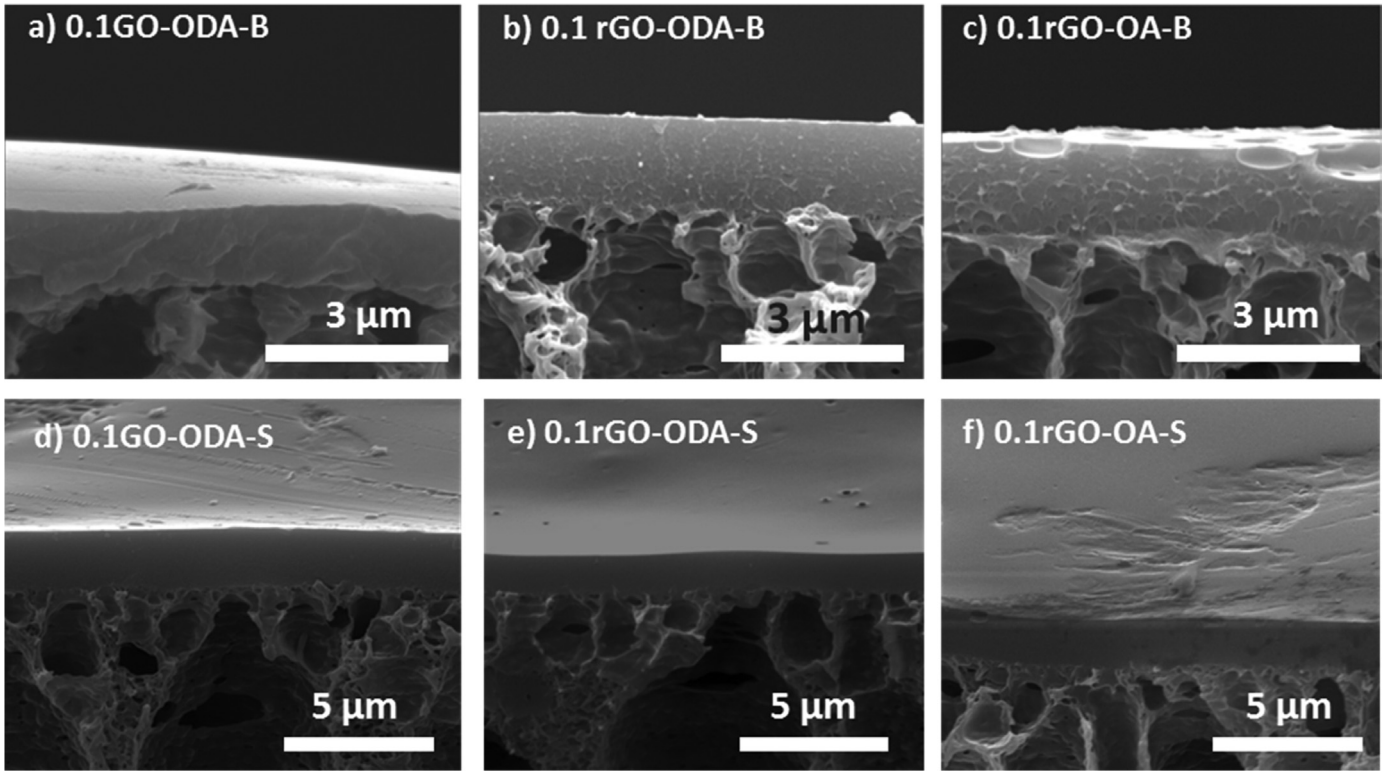

Fig. 4. Cross-sectional SEM images of TFN membrane prepared with graphene-like nanosheets of lateral sizes in the micrometer range: (a) 0.1GO-ODA-B, (b) 0.1rGO-ODA-B, (c) 0.1rGO-OA-B, and TFN membranes containing fillers whose lateral size falls in the nanometer range: (d) 0.1GO-ODA-S, (e) 0.1rGO-ODA-S, (f) 0.1rGO-OA-S.

3.3. TFN membranes

The weight-average molar mass and polydispersity index of the PIM-1 polymer were determined as 123,000 g mol^{-1} and 3.1, respectively, by gel permeation chromatography (GPC).

The concentrations of filler in the membranes were determined through UV–Visible spectroscopy and are presented in Table S1. The code for each membrane is given by the loading (in wt%) and type of filler (GO-ODA, rGO-ODA or rGO-OA) followed by either *B* or *S*, depending on the lateral size of the filler; *B* for big nanosheets (probe sonicated for 10 min), and *S* for small ones (probe sonicated for 8 h). According to these results, the values obtained from UV–Visible spectroscopy are in line with those calculated on the basis of the weighed amounts and concentrations used for the coating process.

Cross-sections of PIM-1-graphene TFN membranes containing 0.1 wt % of filler, as calculated for the coating solutions, are shown in Fig. 4 and confirm the successful preparation of homogenous thin layers on top of PVDF porous substrates through the dip-coating technique. Active layer thicknesses were in the range 1–1.5 µm and the SEM images reveal a homogeneous distribution of the filler in the polymeric matrix with no agglomerates.

Cross sectional TEM measurements were performed to characterize the TFN membranes produced in this work. Fig. 5 shows a 80 nm thin cross section of the TFN membrane 0.1rGO-OA-S and structure analysis, such as high resolution bright field scanning transmission electron microscopy (BF-STEM) and electron diffraction (ED) to demonstrate the presence of the graphene-based nanosheet. Fig. 5(a) shows a BF-STEM image nanosheet and the corresponding ED pattern is displayed and compared to the ED pattern of a PIM only area in Fig. 5(b). PIM has an amorphous structure, which provides diffuse rings in the ED pattern. The graphene based nanosheet is a crystalline material from which we would expect sharper feature -rings, or spots, depending on the geometry. Functionalized rGO nanosheets are known to have higher degree of disorder than highly crystalline graphene flakes, that will make the features observed in the ED pattern more diffuse than in case of bare graphene. On top of that, the ED is probing an area significantly larger than the nanosheet itself and the main contribution to the ED pattern still comes from the amorphous PIM materials. This results in slightly sharper ring in the ED pattern (inset of Fig. 5(b)) and a small peak around 4.7 nm^{-1} ({1010} graphene lattice spacing) on the top of the PIM diffuse contribution, as measured in the intensity profile of the ED pattern (Fig. 5(b)). The high resolution BF-STEM image (inset of Fig. 5(a)) confirms this observation by showing rGO interlayer lattice imaging corresponding to the (0001) graphene lattice spacing of the nanosheet, which means that the nanosheet is observed edge on. Form the BF STEM in Fig. 5(a), it can also be observed that no pores are formed between the filler and the PIM, from which it can be inferred that a good quality interface is formed between both.

The hydrophobicity of the membranes was evaluated by measuring their surface water contact angles. Fig. S5 shows the values obtained for a range of TFN membranes containing the three types of alkyl-functionalized graphene materials (GO-ODA, rGO-ODA, rGO-OA) of lateral sizes in the micrometer range (membrane codes ending -*B*) and in the nanometer range (membrane codes ending -*S*). Pure PIM-1 TFC membranes revealed a contact angle of 92 ± 4°, while the value of the PVDF support on which the thin films were cast was 86 ± 3°. There was not much difference between the contact angles of membranes with big and small fillers, ranging 89 − 100°, although they are slightly higher than those reported in our previous study on freestanding membranes [22]. This might be a consequence of the increased surface roughness of TFN membranes due to the PVDF substrate underneath, as per Wenzel's law. This states that the effect of increased surface roughness is to amplify the intrinsic property of the material which, in this case, is hydrophobicity.

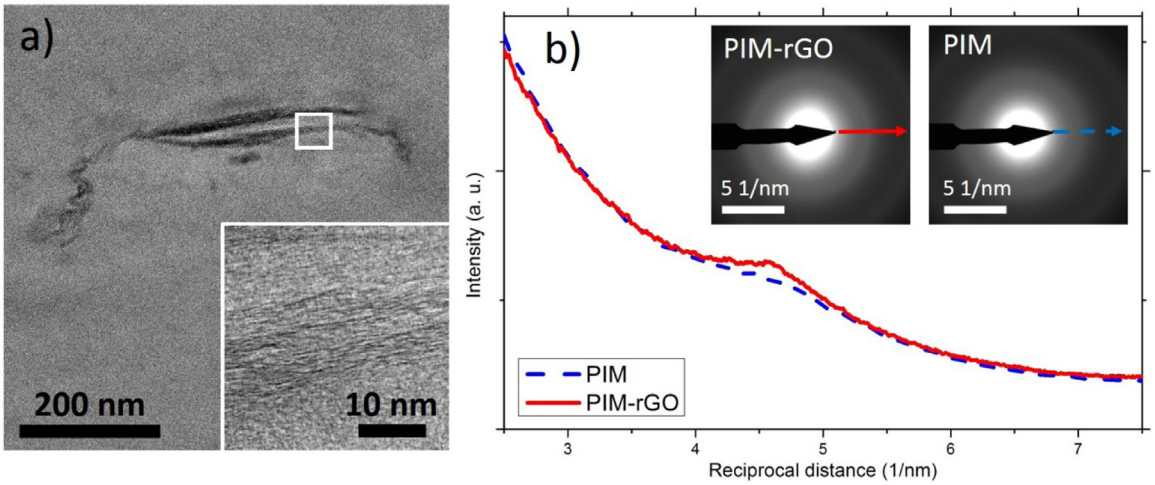

Fig. 5. (a) Cross sectional BF-STEM images showing a rGO-OA-S flake in the TFN membrane 0.1rGO-OA-S. The high resolution BF-STEM image taken from the area marked by white square in (a) is displayed in the inset and shows lattice imaging corresponding to the rGO-OA interlayer spacing. (b) Intensity profile of electron diffraction pattern taken from a PIM-rGO-OA-S area (solid red line) and PIM only (dash blue line) areas. The corresponding electron diffraction patterns are shown in inset.

3.3.1. *Pervaporation performance of TFN membranes*

The TFN membranes were tested for *n*-butanol removal from aqueous solutions via pervaporation at 65 °C using a solution containing 5 wt% of *n*-butanol as feed. The separation performance is evaluated using two parameters: (i) the total flux of solution permeating through the composite membrane, *J,* in units of kg m^{-2} h^{-1}, and (ii) the dimensionless separation factor *β*. *J* accounts for the production rate of the concentrated alcohol solution that is able to go through the membrane per unit area and unit time. *β* represents the weight ratio of alcohol to water in the permeate over the weight ratio in the feed, so higher values of *β* mean higher output of alcohol in the permeate and a more effective separation. Fig. 6 depicts *J* and *β* when micrometer-sized graphene-like materials (probe sonicated for shorter times of 10 min) are used. The same parameters are plotted in Fig. 7 for TFN membranes made with nanometer-sized graphene-like materials (probe sonicated for longer times of 8 h, and therefore smaller). In our previous study, the thickness-normalized total flux for freestanding PIM-1 membranes tested under the same conditions was ~ 70 μm kg m^{-2} h^{-1} [22]. Considering only the apparent thickness of the layers formed on top of the PVDF support (~ 1 μm), one would expected a flux of ca. 70 kg m^{-2} h^{-1} for the thin composite membranes prepared in this work. However, a flux one order of magnitude smaller of 4.3 ± 1.0 kg m^{-2} h^{-1} is obtained for pure PIM-1 TFC membranes, in good agreement with values reported for these type of membranes of about the same thickness [47]. This result suggests that the total permeate flow rate is proportional to the support porosity (the surface porosity of the PVDF supports is in the range 4.2–11.7%). Some penetration of the coating solutions into the PVDF supports during the fabrication process, could increase the overall effective thicknesses, however this is not observed in the SEM pictures presented in Fig. 4. Physical aging is another factor that can contribute to the observed lower flux values, especially because aging in glassy polymers is known to be faster for thin films [54], and it has been reported that PIM-1 even ages in the presence of methanol vapors [55]. On the other hand, the average separation factors reported for freestanding PIM-1 membrane (13.5) [22] and PIM-1 TFC membranes in this work (12.7) are very similar.

The incorporation of graphene nanosheets with lateral sizes in the micrometer-scale decreased the *n*-butanol separation factor as

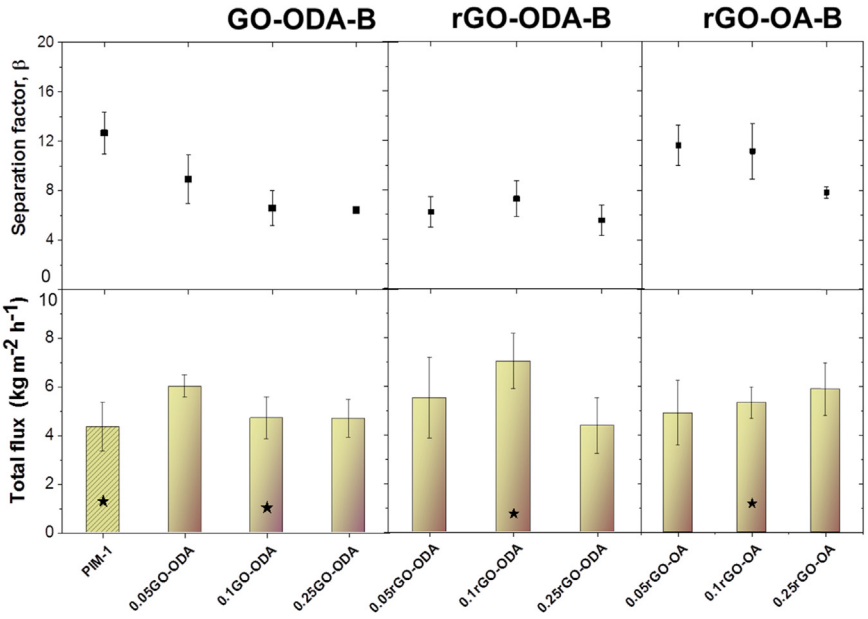

Fig. 6. PV performance of TFN PIM-1/graphene-like membranes with graphene-like flakes of lateral size in the micrometer range (probe sonication time of 10 min). Membranes were all tested at 65 °C using a feed composition 5 wt% *n*-butanol/water, under a downstream pressure of 10 mbar. Separation factors for *n*-butanol (*β*) are displayed in the top graphs, whereas the bars at the bottom represent values of total flux (*J*). Values of *J* and *β* for pure PIM-1 TFC membranes are also included in the graph (patterned bar and point above it). Stars indicate the value of flux obtained for freestanding membranes in our previous publication [22].

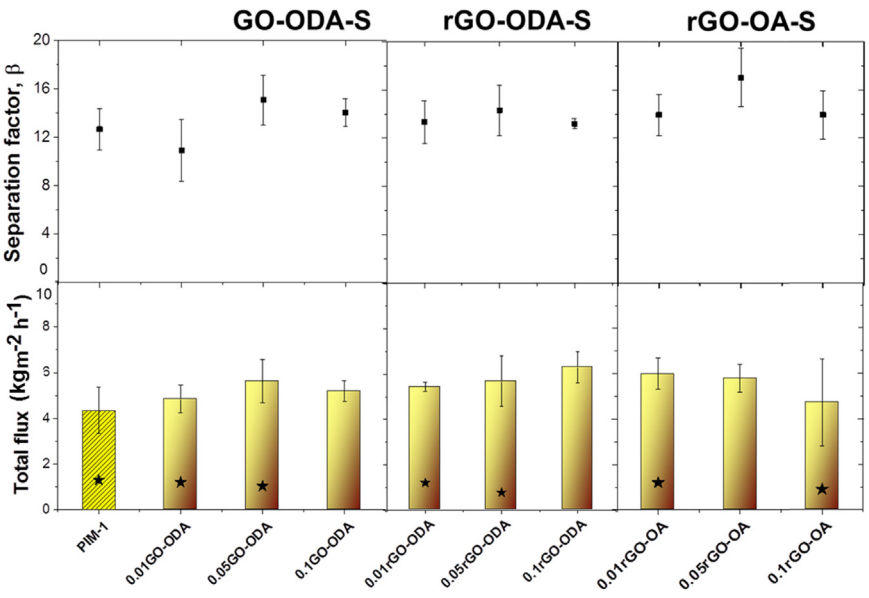

Fig. 7. PV performance of TFN PIM-1/graphene membranes with graphene-like flakes of lateral size in the nanometer range (probe sonication time of 8 h). Membranes were all tested at 65 °C using a feed composition 5 wt% *n*-butanol/water, under a downstream pressure of 10 mbar. Separation factors for *n*-butanol (β) are displayed in the top graphs, whereas the bars at the bottom represent values of total flux (J). Values of J and β for pure PIM-1 TFC membranes are also included in the graph (patterned bar and point above it). Stars indicate the value of flux obtained for freestanding membranes in our previous publication [22].

compared to pure PIM-1 thin film membranes. Considering the thickness of the selective PIM-1-based layers in the TFN membranes and the size of the fillers, it is quite likely that some of them might span the entire thickness of the membrane. Moreover, the expected alignment of the polymer segments with the graphene flakes tends to become more difficult if big graphene flakes are used [56]. If non-selective voids at the polymer-filler interface or agglomerates are created, the performance of the membranes can be compromised. Generally when this happens the separation factor decreases and the flux through the membrane increases. This trend was observed for the majority of the membranes, although for a few of them whose content of filler was in the higher range the flux remained about the same. For the latter the presence of defects might have led to the observed decrease in the separation factor; the impermeability of the graphene-like flakes (i.e. higher tortuosity) in conjunction with a higher flux through non-selective gaps being responsible for the unchanged flux. In our previous study on freestanding membranes, the incorporation of these materials with lateral sizes in the micrometer range led to an enhancement of separation factor to a great extent, reaching 32.9 for a ~ 60 μm thick PIM-1 membrane containing 0.1 wt% rGO-OA [22].

In contrast, when nanometer-sized flakes were incorporated into the polymer thin matrices, the overall performance of the membranes was improved (Fig. 7). This may be attributed to a better polymer-filler interface, and therefore, fewer voids being created [56]. Similarly to our results, Kudasheva *et al.* observed an enhancement in the performance of membranes of the polyimide Matrimid® incorporating smaller (0.53 μm) ordered mesoporous MCM-41 silica spheres, compared to larger (3.1 μm) particles, for water/ethanol separation [17]. They hypothesized this enhancement as an increase in area/volume ratio for smaller particles and a consequent better polymer-filler interface and dispersion. This explanation may also apply to the results in this work for the nanometer-sized fillers containing MMMs. Taking a further look at the available literature, Wang et al. [50] and Rodenas et al. [49] also reported enhanced membrane performance when smaller fillers were incorporated in polyimide matrices. Wang and co-workers justified the enhancement by a better compatibility of smaller silicalite-1 with the PDMS matrix [50]. On the other hand, Rodenas et al. observed a uniform distribution of CuBTC (BTC = 1,3,5-benzenetricarboxylate) nanosheets across the whole membrane, eliminating possible non-selective pathways, as compared to CuBTC crystals [49]. Nonetheless, higher filler loading compromised the overall membrane performance, possibly due to filler aggregation, as also seen by Kudasheva et al. [17]. In our work the best separation performance is obtained for the 0.05rGO-OA-S membrane (nanometer-sized fillers) with a total flux and separation factor of 5.8 ± 0.6 kg m^{-2} h^{-1} and 17.0 ± 2.4, respectively. These slightly higher values as compared to a pristine PIM-1 TFC membrane can be explained by an increase of the *n*-butanol content in the permeate due to a higher affinity of the rGO-OA filler towards this solvent, thus hindering the water sorption [22].

PERVAP® membranes were tested in order to obtain a benchmark value and compare the performance of the thin film nanocomposites fabricated in this study against commercially available films. PERVAP® membranes presented a total flux and separation factor of 3.8 ± 0.9 kg m^{-2} h^{-1} and 16.4 ± 1.3, respectively. Consequently, the best membrane fabricated in this work (0.05rGO-OA-S) presents similar separation performance with a ca. 53% enhancement in yield.

3.3.2. *Effect of the feed composition on the pervaporation performance*

Membranes containing 0.05 wt% of the nanometer-scale fillers were chosen to study the effect of feed concentration and operating temperature on the overall membrane performance. Fig. 8 shows the effect of feed composition on the PV performance of PIM-1, 0.05GO-ODA-S, 0.05rGO-ODA-S and 0.05rGO-OA-S TFN membranes at 65 °C. Aqueous solutions with *n*-butanol concentrations in the range 2 − 5 wt% were used. All membranes show an increase in both flux and separation factor with the increase in *n*-butanol content in the feed. First of all, the organophilic nature of the membranes makes their interaction with *n*-butanol favorable over water, as reported in our previous publication [22]. Furthermore, the membrane swelling degree increases with the *n*-butanol content in the feed, adding free volume and leading consequently to the enhancement of the total flux as also observed in the work by Fouad et al. [57]. In addition, the progressive increase of flux with the increase in *n*-butanol feed content can be due to the enhancement of the driving force across the membrane [16,58]. The increase in *n*-butanol feed content also had a positive effect on the *n*-butanol separation factor. Although both water and *n*-butanol fluxes are enhanced with increasing *n*-butanol feed content, the increase in separation factor is due to the increase in *n*-butanol content in the permeate at a greater extent than water. However, for membrane 0.05rGO-OA-S β is further enhanced due to the observed decrease in water flux, reaching a maximum value at an *n*-butanol feed concentration of 5 wt% (17.0 ± 2.4). This decrease in water flux for membranes containing rGO-OA may be attributed to a lower degree of swelling due to the presence of the rGO-OA-S filler in the PIM-1 matrix. Here the shorter length of the alkyl chain in the rGO-OA fillers can possibly aid in preventing the swelling as compared to longer chains in

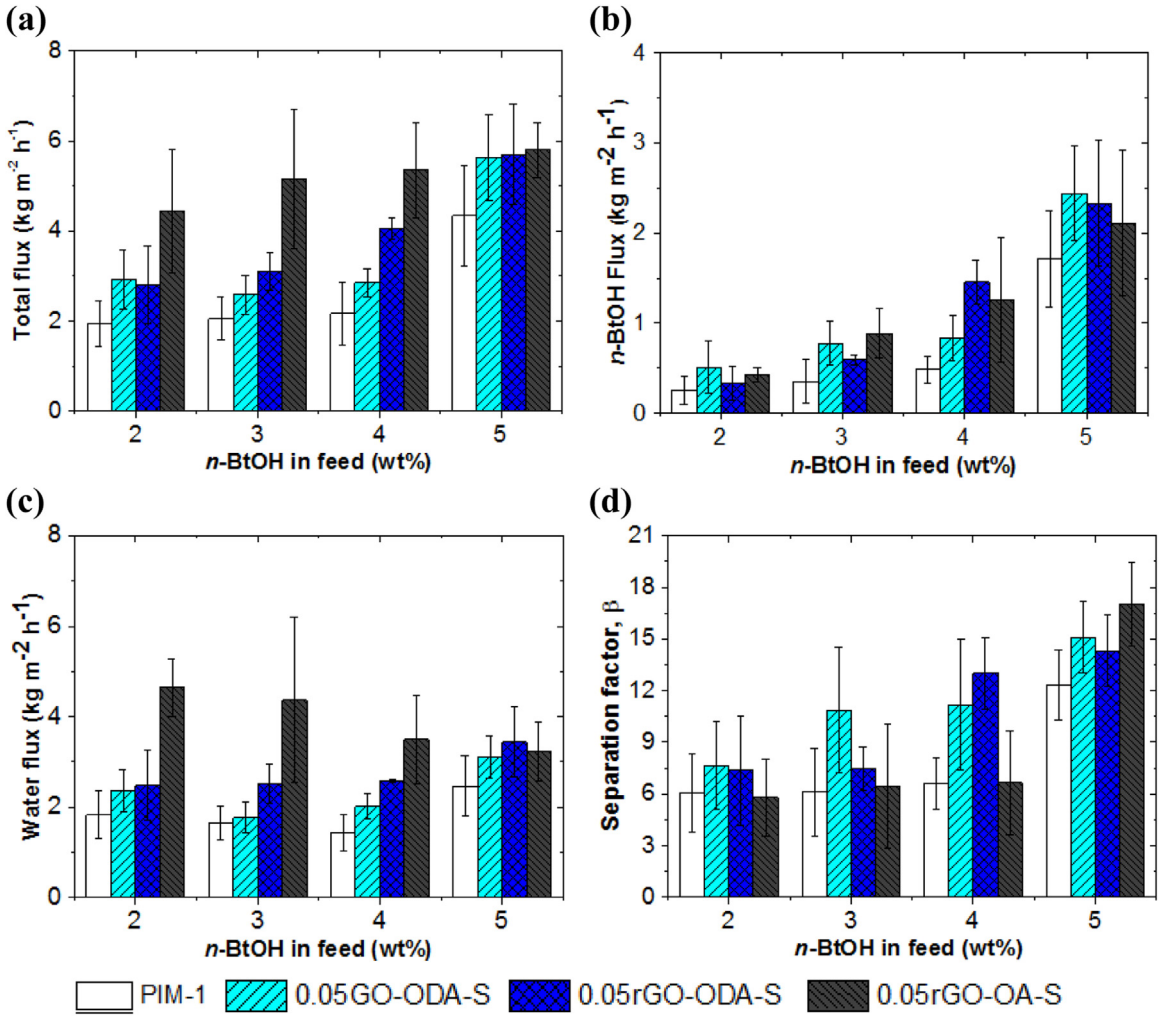

Fig. 8. Effect of the feed composition on the (a) total, (b) *n*-butanol and (c) water fluxes, and (d) separation factor of PIM-1, 0.05GO-ODA-S, 0.05rGO-ODA-S and 0.05rGO-OA-S TFN membranes. All membranes were tested at 65 °C.

GO-ODA and rGO-ODA.

3.3.3. *Effect of the operating temperature on the pervaporation performance*

The effect of temperature on the membrane performance was also investigated, as shown in Fig. 9. Operating temperatures were in the range 35 − 65 °C and a 5 wt% *n*-butanol aqueous solution was used as the feed. All membranes show an increase in total flux as well as partial water and *n*-butanol fluxes when the operating temperature is increased. This can be explained by the fact that the increase in temperature leads to an increase in polymer chain mobility, enlarging the diffusive free volume of the membranes and consequently enhancing their flux [16]. Besides that, the increase in total flux can also be caused by an up to 4-fold increase in difference in vapor pressure which results in higher partial vapor pressure and, therefore, a greater driving force [16]. Moreover, the separation factor is also improved by elevating the operating temperature. Even though an increase of both water and *n*-butanol permeate fluxes is registered, the increase in separation factor is due to an even greater sorption and diffusion of *n*-butanol over water at higher temperatures [59]. The temperature dependence of the permeate flux can be described through the Arrhenius Eq. (3), as follows:

$$J = J_0 exp\left(-\frac{E_a}{RT}\right) \quad (3)$$

where J, J_0, R, T and E_a are the permeation flux (kg m^{-2} h^{-1}), the pre-exponential factor, gas constant (8.314 × 10^{-3} kJ mol^{-1} K^{-1}), absolute feed temperature (K) and apparent activation energy (kJ mol^{-1}) of the specific compound, respectively. According to that, *n*-butanol and water apparent activation energy can be determined by plotting the natural log of the permeation flux of one of the components versus the inverse of the temperature for different operating conditions (Fig. S6). The slope for each curve is $-E_a/R$. The water and *n*-butanol apparent activation energy values for PIM-1, 0.05GO-ODA, 0.05rGO-ODA and 0.05rGO-OA membranes are given in Table 1. The calculated apparent activation energies are always higher for *n*-butanol, which indicates that the *n*-butanol flux is more sensitive to the temperature variation [58]. Therefore, the average separation factor of all membranes increased with the increase in temperature. The 0.05rGO-OA-S membrane achieved the highest separation at 65 °C as it presents the lowest water activation energy among all.

4. Conclusions

In this study, thin film nanocomposite membranes of PIM-1 and functionalized graphene-like fillers were successfully fabricated for *n*-butanol recovery from aqueous solutions. Micrometer- and nanometer-sized GO-ODA, rGO-ODA and rGO-OA flakes were used as fillers; in all cases the flux increased by at least 190% as compared to freestanding membranes of ~ 60 μm in thickness. The use of nanometer-sized flakes led to an enhancement in the separation performance, whereas the incorporation of micrometer-sized ones led to a reduced selectivity towards *n*-butanol as compared to pure PIM-1 membranes. This

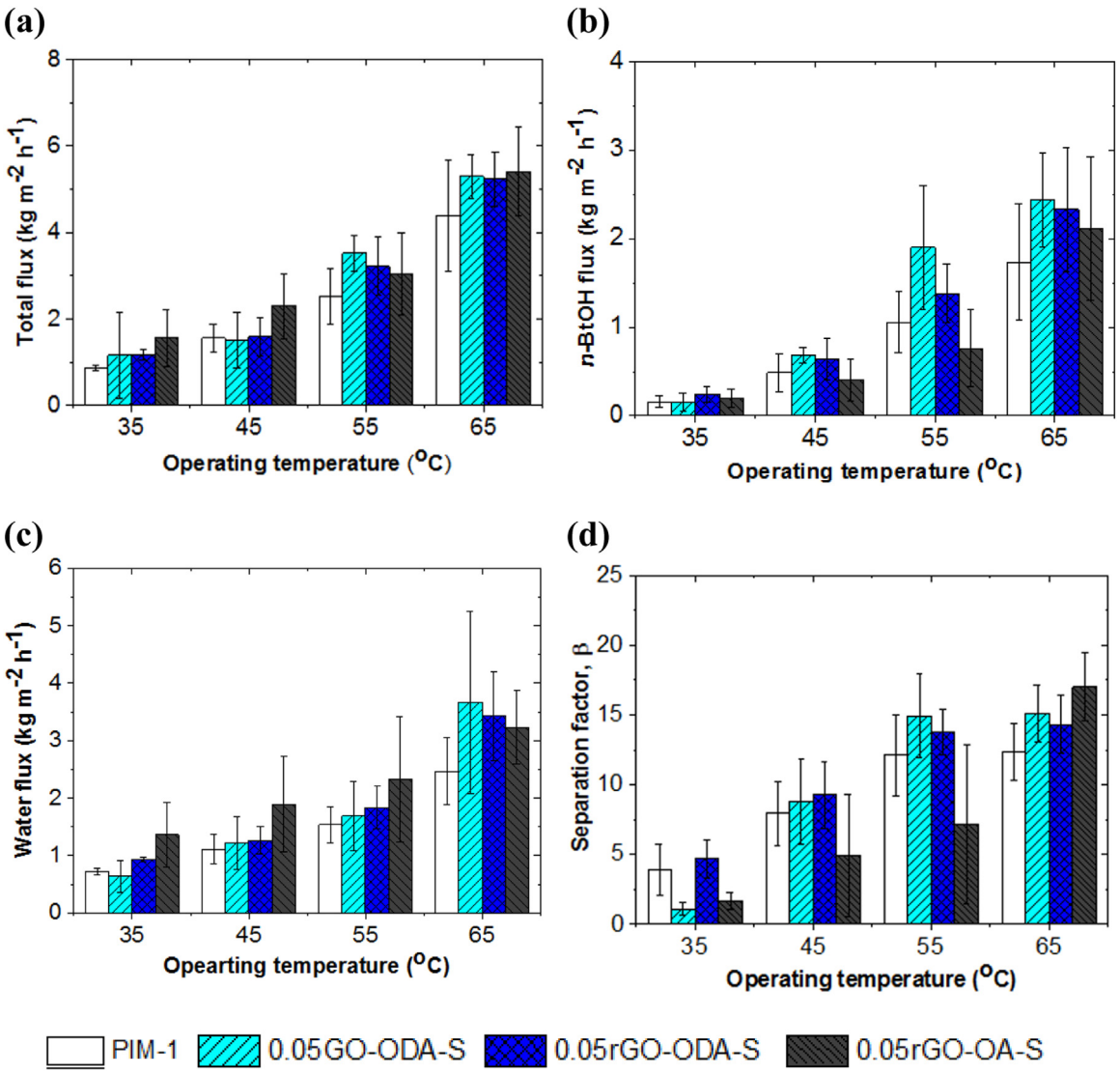

Fig. 9. Effect of the operating temperature on the (a) total, (b) *n*-butanol and (c) water fluxes, and (d) separation factor of PIM-1, 0.05GO-ODA-S, 0.05rGO-ODA-S and 0.05rGO-OA-S TFN membranes. Membranes were tested at 35, 45, 55 and 65 °C using a 5 wt% *n*-butanol aqueous solution as feed.

Table 1
Water and *n*-butanol permeation activation energy values for PIM-1, 0.05GO-ODA, 0.05rGO-ODA and 0.05rGO-OA thin film membranes.

Membranes	$E_{a,\ water}$ (kJ mol^{-1})	$E_{a,\ n\text{-}Butanol}$ (kJ mol^{-1})
PIM-1	34.5	70.6
0.05GO-ODA–S	45.5	85.9
0.05rGO-ODA–S	36.4	65.9
0.05rGO-OA–S	25.6	68.0

suggests that the filler-polymer interface plays an important role in the overall PV performance; when micrometer-sized flakes are used, voids between the polymer and graphene are created, while the use of smaller flakes facilitate their alignment with the polymer segments, decreasing therefore the chance of creating large and non-selective voids. Despite that, the performance of TFN membranes with small flakes seems to be compromised when filler loadings are higher than 0.1 wt%, which can be explained by the effect of agglomeration as the content of filler increases. According to the results obtained, the best separation performance is achieved by a membrane containing 0.05 wt% octyl-functionalized GO of lateral size in the nanometer range. The separation factor reached by this membrane is 17.0 ± 2.4, which represents an improvement of ca. 34% as compared to a pristine PIM-1 thin film composite membrane. From the results it is also suggested that the presence of alkyl chains might also affect the packing of the polymer chains; the short alkyl chain-functionalized filler (rGO-OA) can prevent swelling to a larger extent. In addition, the effects of feed composition and operating temperature were also studied and showed an increase in *n*-butanol flux and separation factor with higher contents of *n*-butanol in the feed and increased operating temperatures.

In summary, our work demonstrates that PIM-1 based TFN membranes containing alkyl-functionalized GO nanosheets are promising candidates for *n*-butanol recovery from aqueous solutions with a ca. 53% enhancement in pervaporative flux as compared to commercial membranes.

Acknowledgments

The authors thank the Engineering and Physical Sciences Research Council EPSRC for funding (EP/K016946/1 and EP/M001342/1). M. Alberto and J. M. Luque-Alled thank to the School of Chemical Engineering and Analytical Science – The University of Manchester for funding their Ph.D studies.

Appendix A. Supporting information

Supplementary data associated with this article can be found in the online version at doi:10.1016/j.memsci.2018.08.050.

References

[1] G. Liu, W. Wei, W. Jin, Pervaporation membranes for biobutanol production, ACS Sustain. Chem. Eng. 2 (2014) 546–560.
[2] A.F. Ismail, P.S. Goh, S.M. Sanip, M. Aziz, Transport and separation properties of carbon nanotube-mixed matrix membrane, Sep. Purif. Technol. 70 (2009) 12–26.
[3] K. Varoon, X.Y. Zhang, B. Elyassi, D.D. Brewer, M. Gettel, S. Kumar, J.A. Lee, S. Maheshwari, A. Mittal, C.Y. Sung, M. Cococcioni, L.F. Francis, A.V. McCormick, K.A. Mkhoyan, M. Tsapatsis, Dispersible exfoliated zeolite nanosheets and their application as a selective membrane, Science 334 (2011) 72–75.
[4] S. Karan, S. Samitsu, X.S. Peng, K. Kurashima, I. Ichinose, Ultrafast viscous permeation of organic solvents through diamond-like carbon nanosheets, Science 335 (2012) 444–447.
[5] R.R. Nair, H.A. Wu, P.N. Jayaram, I.V. Grigorieva, A.K. Geim, Unimpeded permeation of water through helium-leak-tight graphene-based membranes, Science 335 (2012) 442–444.
[6] R.K. Joshi, P. Carbone, F.C. Wang, V.G. Kravets, Y. Su, I.V. Grigorieva, H.A. Wu, A.K. Geim, R.R. Nair, Precise and ultrafast molecular sieving through graphene oxide membranes, Science 343 (2014) 752–754.
[7] J. Abraham, K.S. Vasu, C.D. Williams, K. Gopinadhan, Y. Su, C.T. Cherian, J. Dix, E. Prestat, S.J. Haigh, I.V. Grigorieva, P. Carbone, A.K. Geim, R.R. Nair, Tunable sieving of ions using graphene oxide membranes, Nat. Nanotechnol. 12 (2017) 546 (-+).
[8] H.W. Kim, H.W. Yoon, S.M. Yoon, B.M. Yoo, B.K. Ahn, Y.H. Cho, H.J. Shin, H. Yang, U. Paik, S. Kwon, J.Y. Choi, H.B. Park, Selective gas transport through few-layered graphene and graphene oxide membranes, Science 342 (2013) 91–95.
[9] H. Li, Z.N. Song, X.J. Zhang, Y. Huang, S.G. Li, Y.T. Mao, H.J. Ploehn, Y. Bao, M. Yu, Ultrathin, molecular-sieving graphene oxide membranes for selective hydrogen separation, Science 342 (2013) 95–98.
[10] Q. Yang, Y. Su, C. Chi, C.T. Cherian, K. Huang, V.G. Kravets, F.C. Wang, J.C. Zhang, A. Pratt, A.N. Grigorenko, F. Guinea, A.K. Geim, R.R. Nair, Ultrathin graphene-based membrane with precise molecular sieving and ultrafast solvent permeation, Nat. Mater. 16 (2017) 1198.
[11] Y. Hu, J. Wei, Y. Liang, H. Zhang, X. Zhang, W. Shen, H. Wang, Zeolitic imidazolate framework/graphene oxide hybrid nanosheets as seeds for the growth of ultrathin molecular sieving membranes, Angew. Chem. Int. Ed. 55 (2016) 2048–2052.
[12] Y. Han, Z. Xu, C. Gao, Ultrathin graphene nanofiltration membrane for water purification, Adv. Funct. Mater. 23 (2013) 3693–3700.
[13] K. Goh, W.C. Jiang, H.E. Karahan, S.L. Zhai, L. Wei, D.S. Yu, A.G. Fane, R. Wang, Y. Chen, All-carbon nanoarchitectures as high-performance separation membranes with superior stability, Adv. Funct. Mater. 25 (2015) 7348–7359.
[14] H. Liu, H. Wang, X. Zhang, Facile fabrication of freestanding ultrathin reduced graphene oxide membranes for water purification, Adv. Mater. 27 (2015) 249–254.
[15] L. Huang, J. Chen, T. Gao, M. Zhang, Y. Li, L. Dai, L. Qu, G. Shi, Reduced graphene oxide membranes for ultrafast organic solvent nanofiltration, Adv. Mater. 28 (2016) 8669–8674.
[16] X. Zhuang, X. Chen, Y. Su, J. luo, W. Cao, Y. Wan, Improved performance of PDMS/silicalite-1 pervaporation membranes via designing new silicalite-1 particles, J. Membr. Sci. 493 (2015) 37–45.
[17] A. Kudasheva, S. Sorribas, B. Zornoza, C. Téllez, J. Coronas, Pervaporation of water/ethanol mixtures through polyimide based mixed matrix membranes containing ZIF-8, ordered mesoporous silica and ZIF-8-silica core-shell spheres, J. Chem. Technol. Biotechnol. 90 (2015) 669–677.
[18] S. Liu, G. Liu, X. Zhao, W. Jin, Hydrophobic-ZIF-71 filled PEBA mixed matrix membranes for recovery of biobutanol via pervaporation, J. Membr. Sci. 446 (2013) 181–188.
[19] S. Sorribas, A. Kudasheva, E. Almendro, B. Zornoza, Ó. de la Iglesia, C. Téllez, J. Coronas, Pervaporation and membrane reactor performance of polyimide based mixed matrix membranes containing MOF HKUST-1, Chem. Eng. Sci. 124 (2015) 37–44.
[20] C. Xue, G.-Q. Du, L.-J. Chen, J.-G. Ren, J.-X. Sun, F.-W. Bai, S.-T. Yang, A carbon nanotube filled polydimethylsiloxane hybrid membrane for enhanced butanol recovery, Sci. Rep. 4 (2014) 5925.
[21] M.M. Khan, V. Filiz, G. Bengtson, S. Shishatskiy, M. Rahman, V. Abetz, Functionalized carbon nanotubes mixed matrix membranes of polymers of intrinsic microporosity for gas separation, Nanoscale Res. Lett. 7 (2012) 504.
[22] M. Alberto, J.M. Luque-Alled, L. Gao, M. Iliut, E. Prestat, L. Newman, S.J. Haigh, A. Vijayaraghavan, P.M. Budd, P. Gorgojo, Enhanced organophilic separations with mixed matrix membranes of polymers of intrinsic microporosity and graphene-like fillers, J. Membr. Sci. 526 (2017) 437–449.
[23] Ş.B. Tantekin-Ersolmaz, Ç. Atalay-Oral, M. Tatlıer, A. Erdem-Şenatalar, B. Schoeman, J. Sterte, Effect of zeolite particle size on the performance of polymer–zeolite mixed matrix membranes, J. Membr. Sci. 175 (2000) 285–288.
[24] A. Sabetghadam, B. Seoane, D. Keskin, N. Duim, T. Rodenas, S. Shahid, S. Sorribas, C.L. Guillouzer, G. Clet, C. Tellez, M. Daturi, J. Coronas, F. Kapteijn, J. Gascon, Metal organic framework crystals in mixed-matrix membranes: impact of the filler morphology on the gas separation performance, Adv. Funct. Mater. 26 (2016) 3154–3163.
[25] Q.G. Zhang, C. Deng, F. Soyekwo, Q.L. Liu, A.M. Zhu, Sub-10 nm wide cellulose nanofibers for ultrathin nanoporous membranes with high organic permeation, Adv. Funct. Mater. 26 (2016) 792–800.
[26] S. Karan, Z.W. Jiang, A.G. Livingston, Sub-10 nm polyamide nanofilms with ultrafast solvent transport for molecular separation, Science 348 (2015) 1347–1351.
[27] M.F. Jimenez-Solomon, Q.L. Song, K.E. Jelfs, M. Munoz-Ibanez, A.G. Livingston, Polymer nanofilms with enhanced microporosity by interfacial polymerization, Nat. Mater. 15 (2016) 760.
[28] S. Sorribas, P. Gorgojo, C. Tellez, J. Coronas, A.G. Livingston, High flux thin film nanocomposite membranes based on metal-organic frameworks for organic solvent nanofiltration, J. Am. Chem. Soc. 135 (2013) 15201–15208.
[29] J.Y. Zhu, L.J. Qin, A. Uliana, J.W. Hou, J. Wang, Y.T. Zhang, X. Li, S.S. Yuan, J. Li, M.M. Tian, J.Y. Lin, B. Van der Bruggen, Elevated performance of thin film nanocomposite membranes enabled by modified hydrophilic MOFs for nanofiltration, ACS Appl. Mater. Interfaces 9 (2017) 1975–1986.
[30] D. Ma, S.B. Peh, G. Han, S.B. Chen, Thin-film nanocomposite (TFN) membranes incorporated with super-hydrophilic metal–organic framework (MOF) UiO-66: toward enhancement of water flux and salt rejection, ACS Appl. Mater. Interfaces 9 (2017) 7523–7534.
[31] J. Wang, Y. Wang, Y. Zhang, A. Uliana, J. Zhu, J. Liu, B. Van der Bruggen, Zeolitic imidazolate framework/graphene oxide hybrid nanosheets functionalized thin film nanocomposite membrane for enhanced antimicrobial performance, ACS Appl. Mater. Interfaces 8 (2016) 25508–25519.
[32] S.G. Kim, D.H. Hyeon, J.H. Chun, B.-H. Chun, S.H. Kim, Novel thin nanocomposite RO membranes for chlorine resistance, Desalin. Water Treat. 51 (2013) 6338–6345.
[33] L. Shen, S. Xiong, Y. Wang, Graphene oxide incorporated thin-film composite membranes for forward osmosis applications, Chem. Eng. Sci. 143 (2016) 194–205.
[34] W.-S. Hung, C.-L. Lai, Q. An, M. De Guzman, T.-J. Shen, Y.-H. Huang, K.-C. Chang, C.-H. Tsou, C.-C. Hu, K.-R. Lee, A study on high-performance composite membranes comprising heterogeneous polyamide layers on an electrospun substrate for ethanol dehydration, J. Membr. Sci. 470 (2014) 513–523.
[35] D. Wu, J. Martin, J. Du, Y. Zhang, D. Lawless, X. Feng, Thin film composite membranes comprising of polyamide and polydopamine for dehydration of ethylene glycol by pervaporation, J. Membr. Sci. 493 (2015) 622–635.
[36] J. Niemistö, W. Kujawski, R.L. Keiski, Pervaporation performance of composite poly (dimethyl siloxane) membrane for butanol recovery from model solutions, J. Membr. Sci. 434 (2013) 55–64.
[37] L. Hao, K.-S. Liao, T.-S. Chung, Photo-oxidative PIM-1 based mixed matrix membranes with superior gas separation performance, J. Mater. Chem. A 3 (2015) 17273–17281.
[38] Y. Kinoshita, K. Wakimoto, A.H. Gibbons, A.P. Isfahani, H. Kusuda, E. Sivaniah, B. Ghalei, Enhanced PIM-1 membrane gas separation selectivity through efficient dispersion of functionalized POSS fillers, J. Membr. Sci. 539 (2017) 178–186.
[39] T. Mitra, R.S. Bhavsar, D.J. Adams, P.M. Budd, A.I. Cooper, PIM-1 mixed matrix membranes for gas separations using cost-effective hypercrosslinked nanoparticle fillers, Chem. Commun. 52 (2016) 5581–5584.
[40] S.V. Adymkanov, Y.P. Yampol'skii, A.M. Polyakov, P.M. Budd, K.J. Reynolds, N.B. McKeown, K.J. Msayib, Pervaporation of alcohols through highly permeable PIM-1 polymer films, Polym. Sci. Ser. A 50 (2008) 444–450.
[41] P.M. Budd, E.S. Elabas, B.S. Ghanem, S. Makhseed, N.B. McKeown, K.J. Msayib, C.E. Tattershall, D. Wang, Solution-Processed, Organophilic Membrane Derived from a Polymer of Intrinsic Microporosity, Adv. Mater. 16 (2004) 456–459.
[42] P. Gorgojo, S. Karan, H.C. Wong, M.F. Jimenez-Solomon, J.T. Cabral, A.G. Livingston, Ultrathin polymer films with intrinsic microporosity: anomalous solvent permeation and high flux membranes, Adv. Funct. Mater. 24 (2014) 4729–4737.
[43] D. Fritsch, P. Merten, K. Heinrich, M. Lazar, M. Priske, High performance organic solvent nanofiltration membranes: development and thorough testing of thin film composite membranes made of polymers of intrinsic microporosity (PIMs), J. Membr. Sci. 401 (2012) 222–231.
[44] M.L. Jue, V. Breedveld, R.P. Lively, Defect-free PIM-1 hollow fiber membranes, J. Membr. Sci. 530 (2017) 33–41.
[45] S. Sorribas, M. Tamaddondar, P.M. Budd, 1.9 membranes made of polymers of intrinsic microporosity (PIMs), Comprehensive Membrane Science and Engineering, Second ed., Elsevier, Oxford, 2017, pp. 216–235.
[46] M. Žák, M. Klepic, L.Č. Štastná, Z. Sedláková, H. Vychodilová, Š. Hovorka, K. Friess, A. Randová, L. Brožová, J.C. Jansen, M.R. Khdhayyer, P.M. Budd, P. Izák, Selective removal of butanol from aqueous solution by pervaporation with a PIM-1 membrane and membrane aging, Sep. Purif. Technol. 151 (2015) 108–114.
[47] L. Gao, M. Alberto, P. Gorgojo, G. Szekely, P.M. Budd, High-flux PIM-1/PVDF thin film composite membranes for 1-butanol/water pervaporation, J. Membr. Sci. 529 (2017) 207–214.
[48] H. Yin, A. Khosravi, L. O'Connor, A.Q. Tagaban, L. Wilson, B. Houck, Q. Liu, M.L. Lind, Effect of ZIF-71 particle size on free-standing ZIF-71/PDMS composite membrane performances for ethanol and 1-Butanol removal from water through pervaporation, Ind. Eng. Chem. Res. 56 (2017) 9167–9176.
[49] T. Rodenas, I. Luz, G. Prieto, B. Seoane, H. Miro, A. Corma, F. Kapteijn, F.X. Llabrés i Xamena, J. Gascon, Metal–organic framework nanosheets in polymer composite materials for gas separation, Nat. Mater. 14 (2015) 48–55.
[50] N. Wang, J. Liu, J. Li, J. Gao, S. Ji, J.-R. Li, Tuning properties of silicalite-1 for enhanced ethanol/water pervaporation separation in its PDMS hybrid membrane, Microporous Mesoporous Mater. 201 (2015) 35–42.
[51] N.Y. Du, J.S. Song, G.P. Robertson, I. Pinnau, M.D. Guiver, Linear high molecular weight ladder polymer via fast polycondensation of 5,5',6,6'-tetrahydroxy-3,3,3',3'-tetramethylspirobisindane with 1,4-dicyanotetrafluorobenzene, Macromol. Rapid Commun. 29 (2008) 783–788.
[52] J.P. Rourke, P.A. Pandey, J.J. Moore, M. Bates, I.A. Kinloch, R.J. Young,

N.R. Wilson, The real graphene oxide revealed: stripping the oxidative debris from the graphene-like sheets, Angew. Chem. Int. Ed. 50 (2011) 3173–3177.
[53] E. Fontananova, J.C. Jansen, A. Cristiano, E. Curcio, E. Drioli, Effect of additives in the casting solution on the formation of PVDF membranes, Desalination 192 (2006) 190–197.
[54] Y. Huang, D.R. Paul, Effect of film thickness on the gas-permeation characteristics of glassy polymer membranes, Ind. Eng. Chem. Res. 46 (2007) 2342–2347.
[55] K. Pilnacek, O. Vopicka, M. Lanc, M. Dendisova, M. Zgazar, P.M. Budd, M. Carta, R. Malpass-Evans, N.B. McKeown, K. Friess, Aging of polymers of intrinsic microporosity tracked by methanol vapour permeation, J. Membr. Sci. 520 (2016) 895–906.
[56] A. Gonciaruk, K. Althumayri, W.J. Harrison, P.M. Budd, F.R. Siperstein, PIM-1/graphene composite: a combined experimental and molecular simulation study, Microporous Mesoporous Mater. 209 (2015) 126–134.
[57] E.A. Fouad, X. Feng, Use of pervaporation to separate butanol from dilute aqueous solutions: effects of operating conditions and concentration polarization, J. Membr. Sci. 323 (2008) 428–435.
[58] X. Wang, J. Chen, M. Fang, T. Wang, L. Yu, J. Li, ZIF-7/PDMS mixed matrix membranes for pervaporation recovery of butanol from aqueous solution, Sep. Purif. Technol. 163 (2016) 39–47.
[59] M. Hu, L. Gao, W. Fu, X. Liu, F. Huang, Y. Luo, C. Huang, High-performance interpenetrating polymer network polyurethane pervaporation membranes for butanol recovery, J. Chem. Technol. Biotechnol. 90 (2015) 2195–2207.